Density dependencies of interaction strengths and their influences on nuclear matter and neutron stars in relativistic mean field theory

S. F. Ban,[1] J. Li,[1,2] S. Q. Zhang,[1] H. Y. Jia,[1,3] J. P. Sang,[2] and J. Meng[1,4,5,*]
[1]*School of Physics, Peking University, Beijing 100871, China*
[2]*College of Physics and Technology, Wuhan University, Wuhan 430072, China*
[3]*College of Science, Southwest Jiaotong University, Chengdou 610031, China*
[4]*Institute of Theoretical Physics, Chinese Academy of Science, Beijing 100080, China*
[5]*Center of Theoretical Nuclear Physics, National Laboratory of Heavy Ion Accelerator, Lanzhou 730000, China*
(Received 29 August 2003; published 28 April 2004)

The density dependencies of various effective interaction strengths in the relativistic mean field are studied and carefully compared for nuclear matter and neutron stars. The influences of different density dependencies are presented and discussed on mean field potentials, saturation properties for nuclear matter, equations of state, maximum masses, and corresponding radii for neutron stars. Though the interaction strengths and the potentials given by various interactions are quite different in nuclear matter, the differences of saturation properties are subtle, except for NL2 and TM2, which are mainly used for light nuclei, while the properties by various interactions for pure neutron matter are quite different. To get an equation of state for neutron matter without any ambiguity, it is necessary to constrain the effective interactions either by microscopic many-body calculations for the neutron matter data or the data of nuclei with extreme isospin. For neutron stars, the interaction with large interaction strengths give strong potentials and large Oppenheimer-Volkoff (OV) mass limits. The density-dependent interactions DD-ME1 and TW-99 favor a large neutron population due to their weak ρ-meson field at high densities. The OV mass limits calculated from different equations of state are $2.02-2.81M_{\odot}$, and the corresponding radii are 10.78–13.27 km. After the inclusion of the hyperons, the corresponding values become $1.52-2.06M_{\odot}$ and 10.24–11.38 km.

DOI: 10.1103/PhysRevC.69.045805 PACS number(s): 21.30.Fe, 21.60.Jz, 21.65.+f, 26.60.+c

I. INTRODUCTION

A widely used and successful approach for nuclear matter and finite nuclei is the mean field theory employing effective interactions. The mean field theory includes nonrelativistic mean field theory with effective nucleon-nucleon interactions such as Skyrme or Gogny, and the relativistic mean field (RMF) theory. In a certain sense, the RMF theory is more fundamental as it starts from a phenomenological hadronic field theory with strongly interacting baryons and mesons as degrees of freedom [1]. It has been used not only for describing the properties of nuclei near the valley of stability successfully [2], but also for predicting the properties of exotic nuclei with large neutron or proton excess [3,4]. In the mean field theory, the effective interactions are adjusted to various properties of nuclear matter and finite nuclei. In recent years, a number of effective interactions of meson-baryon couplings based on the RMF theory have been developed, including nonlinear self-couplings for the σ-meson and/or ω-meson, such as NL1, NL2 [5], NL3 [6], NLSH [7], TM1, and TM2 [8]. However, these nonlinear interactions have problems of stability at high densities, as well as the question of their physical foundation [5]. A more natural alternative is to introduce the density dependence in the couplings [9]. Based on the Dirac-Brueckner calculations, Typel and Wolter proposed the density-dependent effective interaction TW-99 and expected that the model could be reasonably extrapolated to extreme conditions of isospin and/or density [9]. Along this line, Nikšić *et al.* developed another effective interaction DD-ME1 [10]. In this paper, we will analyze the density dependencies of various effective interactions including both the nonlinear and density-dependent versions in the RMF theory and investigate their influences on properties of nuclear matter and neutron stars.

The existence of neutron stars was predicted following the discovery of neutron. In 1934, Baade and Zwicky suggested that neutron stars could be formed in "supernovae" [11]. The radio pulsars discovered by Bell and Hewith in 1967 [12] were identified as rotating neutron stars by Pacini [13] and Gold [14]. The first theoretical calculation of neutron stars was performed by Oppenheimer and Volkoff [15], and independently by Tolman [16]. In their calculation the neutron stars were assumed as gravitationally bound states of neutron Fermi gas. Recent progress on the study of neutron stars can be found in Refs. [17,18] and references therein.

The physics of neutron stars has offered an intriguing interplay between nuclear processes and astrophysical observation, and has become a hot topic in nuclear physics and astrophysics. The neutron stars exhibit conditions far from those encountered on the earth. The neutron star models including various so-called realistic equations of state have resulted in the following general picture for the interior of neutron star. The surface of neutron star is a solid crust of thickness about 1 km, which is mainly made up of nuclei and free electrons. Inside the crust, charge-neutral neutron star mainly consists of neutrons together with a small concentration of protons and electrons in equal number. Proton and

*Email address: mengj@pku.edu.cn

electron densities increase with total baryon density, and the μ^-, π, K mesons and other baryons (e.g., hyperons) as well as a phase transition from baryon degrees of freedom to quark matter will appear [18].

The equation of state (EOS) is essential to understand the structure and properties of neutron stars. The EOS determines properties such as the mass range, the mass-radius relationship, the crust thickness, the cooling rate, and even the energy released in a supernova explosion. Usually, the EOS is obtained by extrapolating the theory, which is developed mainly for normal nuclear matter, to nuclear matter with extreme high isospin and high densities. Unfortunately, such extrapolation is always model dependent. The RMF theory has proved to be very successful in describing the properties of nuclear matter and finite nuclei [1,2], rotation nuclei [2], nuclei far from β stability [3,4], and magnetic rotation [19], etc. Based on the RMF theory, there are also many studies on neutron stars and strange nuclear matter with effective interactions including nonlinear self-couplings for scalar and vector mesons [17,20–30].

In this paper, the density dependencies of various effective interaction strengths in the RMF theory are studied and compared for nuclear matter and neutron stars. The corresponding influences of different density dependencies for effective interactions are presented and discussed on mean field potentials, saturation properties for nuclear matter, EOS, maximum masses, and corresponding radii for neutron stars. In Sec. II, a brief description of the RMF theory in nuclear matter and neutron stars is presented. The results and discussions are given in the following section. In the last section, we give a brief summary.

II. A SKETCH OF THE RMF THEORY IN NUCLEAR MATTER AND NEUTRON STARS

The details of RMF theory can be found in a number of reviews [1,2,17]. The RMF theory starts from an effective Lagrangian density with baryons, mesons (σ, ω and ρ), and photons as degrees of freedom ($\hbar=c=1$):

$$\begin{aligned}\mathcal{L} = \sum_B \bar{\psi}_B \Big[& i\gamma^\mu\partial_\mu - m_B - g_{\sigma B}\sigma - g_{\omega B}\gamma^\mu\omega_\mu - g_{\rho B}\gamma^\mu\boldsymbol{\tau}_B\cdot\boldsymbol{\rho}_\mu \\ & - e\gamma^\mu A_\mu \frac{1-\tau_{3B}}{2}\Big]\psi_B + \frac{1}{2}\partial_\mu\sigma\partial^\mu\sigma - \frac{1}{2}m_\sigma^2\sigma^2 - U(\sigma) \\ & - \frac{1}{4}\omega_{\mu\nu}\omega^{\mu\nu} + \frac{1}{2}m_\omega^2\omega_\mu\omega^\mu + U(\omega) - \frac{1}{4}\boldsymbol{\rho}_{\mu\nu}\boldsymbol{\rho}^{\mu\nu} + \frac{1}{2}m_\rho^2\boldsymbol{\rho}_\mu\boldsymbol{\rho}^\mu \\ & - \frac{1}{4}A_{\mu\nu}A^{\mu\nu}, \end{aligned} \tag{1}$$

where the Dirac spinor ψ_B denotes the baryon B with mass m_B and isospin τ_B. The sum on B is over protons, neutrons and hyperons ($\Lambda,\Sigma^\pm,\Sigma^0,\Xi^-,\Xi^0$, *et al.*) in this paper. The scalar sigma (σ) and vector omega (ω) offer medium-range attractive and short-range repulsive interactions, respectively, and the isospin vector rho ($\boldsymbol{\rho}$) provides the necessary isospin asymmetry. Their masses are denoted by m_σ, m_ω, and m_ρ. The corresponding meson-baryon coupling constants are $g_{\sigma B}$, $g_{\omega B}$, and $g_{\rho B}$, respectively. $\boldsymbol{\tau}_B$ is the isospin of baryon B and τ_{3B} is its three-component. The nonlinear self-couplings for σ and ω mesons are, respectively,

$$U(\sigma) = \frac{1}{3}g_2\sigma^3 + \frac{1}{4}g_3\sigma^4, \quad U(\omega) = \frac{1}{4}c_3(\omega^\mu\omega_\mu)^2, \tag{2}$$

with the self-coupling constants g_2, g_3, and c_3. The field tensors $\omega_{\mu\nu}$, $\boldsymbol{\rho}_{\mu\nu}$, and $A_{\mu\nu}$ are for ω-meson, ρ-meson, and photon, respectively.

The parametrization of the interaction in the RMF theory is obtained by fitting the properties of nuclear matter and some finite nuclei. Instead of the self-coupling of the meson fields, Typel and Wolter proposed the density dependencies of the couplings in the RMF theory [9], i.e., the coupling constant $g_{\sigma(\omega)B}$ of the $\sigma(\omega)$ meson is replaced by

$$g_{\sigma(\omega)B}(\rho) = g_{\sigma(\omega)B}(\rho_0) f_{\sigma(\omega)}(x), \tag{3}$$

where

$$f_{\sigma(\omega)}(x) = a_{\sigma(\omega)}\frac{1 + b_{\sigma(\omega)}(x + d_{\sigma(\omega)})^2}{1 + c_{\sigma(\omega)}(x + d_{\sigma(\omega)})^2} \tag{4}$$

is a function of $x=\rho/\rho_0$, with the vector density $\rho=\sqrt{j_\mu j^\mu}$, $j_\mu=\Sigma_B\,\bar{\psi}_B\gamma_\mu\psi_B$, and the saturation density of nuclear matter ρ_0. The eight real parameters in Eq. (4) are not independent. The five constraints $f_{\sigma(\omega)}(1)=1$, $f''_{\sigma(\omega)}(0)=0$, and $f''_\sigma(1)=f''_\omega(1)$ reduce the number of independent parameters to three. The density-dependent ρ-meson coupling constant $g_{\rho B}$ is introduced as,

$$g_{\rho B}(\rho) = g_{\rho B}(\rho_0)\exp[-a_\rho(x-1)] \tag{5}$$

with two parameters a_ρ and $g_{\rho B}(\rho_0)$.

The equations of motion for baryons and mesons can be derived from the Lagrangian density in Eq. (1). In the following, we present only the case for the density-dependent couplings. The equations for nonlinear couplings can be obtained easily by adding the nonlinear self-couplings of the mesons and neglecting the density dependencies of the coupling constants.

The equations of motion for baryons are

$$\left[\gamma^\mu\left(i\partial_\mu - g_{\omega B}\omega_\mu - g_{\rho B}\boldsymbol{\tau}_B\cdot\boldsymbol{\rho}_\mu - e\frac{1-\tau_{3B}}{2}A_\mu - \Sigma^R_{\mu B}\right) - m_B^*\right]\psi_B = 0, \tag{6}$$

where the effective mass $m_B^*=m_B+g_{\sigma B}\sigma$, and $\Sigma_{\mu B}^R$ is a "rearrangement" term due to the density dependencies of the couplings:

$$\Sigma_{\mu B}^R=\frac{j_\mu}{\rho}\left(\frac{\partial g_{\omega B}}{\partial\rho}\bar{\psi}_B\gamma^\nu\psi_B\omega_\nu+\frac{\partial g_{\rho B}}{\partial\rho}\bar{\psi}_B\gamma^\nu\boldsymbol{\tau}_B\psi_B\boldsymbol{\rho}_\nu+\frac{\partial g_{\sigma B}}{\partial\rho}\bar{\psi}_B\psi_B\sigma\right). \tag{7}$$

The field equations for mesons and photons are, respectively,

$$(\partial^\mu\partial_\mu+m_\sigma^2)\sigma=-\sum_B g_{\sigma B}\bar{\psi}_B\psi_B, \tag{8}$$

$$\partial_\mu\omega^{\mu\nu}+m_\omega^2\omega^\nu=\sum_B g_{\omega B}\bar{\psi}_B\gamma^\nu\psi_B, \tag{9}$$

$$\partial_\mu\boldsymbol{\rho}^{\mu\nu}+m_\rho^2\boldsymbol{\rho}^\nu=\sum_B g_{\rho B}\bar{\psi}_B\gamma^\nu\boldsymbol{\tau}_B\psi_B+g_{\rho B}\boldsymbol{\rho}_\mu\times\boldsymbol{\rho}^{\mu\nu}, \tag{10}$$

$$\partial_\mu A^{\mu\nu}=e\bar{\psi}\gamma^\nu\frac{1-\tau_{3B}}{2}\psi. \tag{11}$$

A. Nuclear matter

For infinite nuclear matter, introducing the mean field approximation, i.e., the meson fields are replaced by their mean values, and neglecting the coulomb field, the baryon wave function is the eigenstate of momentum k, and the source currents $\bar{\psi}_B\psi_B$ and $\bar{\psi}_B\gamma^\nu\psi_B$ in Eqs. (8)–(10) are independent of the spatial coordinate x. Thus the equations of motion can be simplified as

$$[\gamma^\mu(k_\mu-g_{\omega B}\omega_\mu-g_{\rho B}\boldsymbol{\tau}_B\cdot\boldsymbol{\rho}_\mu-\Sigma_{\mu B}^R)-m_B^*]\psi_B(k)=0, \tag{12}$$

$$m_\sigma^2\sigma=-g_{\sigma B}\rho_s, \tag{13}$$

$$m_\omega^2\omega_0=g_{\omega B}\rho, \tag{14}$$

$$m_\rho^2\rho_{0,3}=\sum_B g_{\rho B}\tau_{3B}\rho_B. \tag{15}$$

For the nonlinear self-coupling effective interactions, the corresponding terms $-U'(\sigma)$ and $-U'(\omega_0)$ should be taken into account in the Eqs. (13) and (14), respectively.

The eigenvalues of the Dirac equation for baryons in Eq. (12) are obtained as

$$e_B(k)=g_{\omega B}\omega_0+g_{\rho B}\tau_{3B}\rho_{0,3}+\Sigma_{0B}^R+\sqrt{k^2+m_B^{*2}}, \tag{16}$$

where Σ_{0B}^R is the time component of the rearrangement term. The baryon vector density ρ and scalar density ρ_s are, respectively,

$$\rho=\sum_B\langle\bar{\psi}_B\gamma^0\psi_B\rangle=\sum_B\rho_B=\sum_B\frac{k_B^3}{3\pi^2}, \tag{17}$$

$$\rho_s=\sum_B\langle\bar{\psi}_B\psi_B\rangle=\sum_B\rho_{sB}=\frac{1}{\pi^2}\sum_B\int_0^{k_B}k^2dk\frac{m_B^*}{\sqrt{k^2+m_B^{*2}}}, \tag{18}$$

where k_B denotes the Fermi momentum of baryon B, and the no-sea approximation has been used.

The energy density and pressure of nuclear matter are, respectively,

$$\varepsilon=\frac{1}{2}m_\sigma^2\sigma^2+\frac{1}{2}m_\omega^2\omega_0^2+\frac{1}{2}m_\rho^2\rho_{0,3}^2+\frac{1}{\pi^2}\sum_B\int_0^{k_B}k^2dk\sqrt{k^2+m_B^{*2}}, \tag{19}$$

$$P=-\frac{1}{2}m_\sigma^2\sigma^2+\frac{1}{2}m_\omega^2\omega_0^2+\frac{1}{2}m_\rho^2\rho_{0,3}^2+\sum_B\rho_B\Sigma_{0B}^R+\frac{1}{3\pi^2}\sum_B\int_0^{k_B}\frac{k^4}{\sqrt{k^2+m_B^{*2}}}dk. \tag{20}$$

B. Neutron stars

The charge-neutral neutron stars includes not only neutrons and protons, but also leptons λ (mainly e^- and μ^-) in equal number to protons and also hyperons at high densities. The Lagrangian density for neutron stars is similar to Eq. (1), except an additional term for leptons:

$$\mathcal{L}_\lambda=\sum_{\lambda=e^-,\mu^-}\bar{\psi}_\lambda(i\gamma^\mu\partial_\mu-m_\lambda)\psi_\lambda, \tag{21}$$

Introducing the mean field and no-sea approximation, the equations of motion for baryons and mesons can be derived, and the corresponding energy eigenvalues, baryon density, and scalar density can be obtained for neutron stars, similar to those for the nuclear matter. The equations of motion for electron and μ^- are free Dirac equations and their densities can be expressed in terms of their corresponding Fermi momenta as $\rho_\lambda=k_\lambda^3/(3\pi^2)$.

The chemical potentials μ_B for the baryons B are the energy eigenvalues of the Dirac equation: $\mu_B=\varepsilon_B(k)$. The chemical potentials μ_λ for the leptons are the solutions of their equations of motion: $\mu_\lambda=\sqrt{k_\lambda^2+m_\lambda^2}$. In neutron stars, the chemical equilibrium conditions are:

$$\mu_B=b_B\mu_n-q_B\mu_e,\quad \mu_\mu=\mu_e, \tag{22}$$

where b_B and q_B denote baryon charge and electronic charge of baryon B, μ_n, μ_e, and μ_μ are the chemical potentials for neutron, electron, and μ^-, respectively. The baryon number conservation and charge-neutral conditions are given by

$$\rho=\sum_B\rho_B=\sum_B\frac{b_Bk_B^3}{3\pi^2}, \tag{23}$$

$$Q=\sum_B Q_B+\sum_\lambda Q_\lambda=\sum_B\frac{q_Bk_B^3}{3\pi^2}-\sum_\lambda\frac{k_\lambda^3}{3\pi^2}=0. \tag{24}$$

The energy density and pressure for neutron stars are, respectively,

$$\varepsilon = \frac{1}{2}m_\sigma^2\sigma^2 + \frac{1}{2}m_\omega^2\omega_0^2 + \frac{1}{2}m_\rho^2\rho_{0,3}^2 + \frac{1}{\pi^2}\sum_B \int_0^{k_B} k^2 dk\sqrt{k^2 + m_B^{*2}} + \frac{1}{\pi^2}\sum_{\lambda=e^-,\mu^-}\int_0^{k_\lambda} k^2 dk\sqrt{k^2 + m_\lambda^2}, \quad (25)$$

$$P = -\frac{1}{2}m_\sigma^2\sigma^2 + \frac{1}{2}m_\omega^2\omega_0^2 + \frac{1}{2}m_\rho^2\rho_{0,3}^2 + \sum_B \rho_B\Sigma_{0B}^R + \frac{1}{3\pi^2}\sum_B \int_0^{k_B} \frac{k^4}{\sqrt{k^2 + m_B^{*2}}}dk + \frac{1}{3\pi^2}\sum_{\lambda=e^-,\mu^-}\int_0^{k_\lambda} dk\frac{k^4}{\sqrt{k^2 + m_\lambda^2}}. \quad (26)$$

III. RESULTS AND DISCUSSIONS

For nuclear matter, Eqs. (13)–(18) provide a set of coupled transcendental relations defining the meson fields and energy eigenvalues. The list of unknowns is

$$\rho, \quad k_B, \quad \rho_s, \quad g_{\omega B}, \quad g_{\sigma B}, \quad g_{\rho B}, \quad \sigma, \quad \omega_0, \quad \rho_{0,3}, \quad \varepsilon_B(k).$$

For a given baryon density ρ and the asymmetry of the nuclear matter $t=(\rho_n-\rho_p)/\rho$, we can get the coupling constants $g_{\sigma B}$, $g_{\omega B}$, and $g_{\rho B}$ from Eqs. (3)–(5), as well as the neutron density ρ_n and proton density ρ_p, and of course their corresponding Fermi momenta k_n and k_p. The ω and ρ fields can be obtained by Eqs. (14) and (15) and the σ field can be solved from Eqs. (13) and (18) by iteration.

The properties of neutron stars can be obtained by solving the Eqs. (13)–(18) and (22)–(24) by the following procedures.

(1) For a given baryon density ρ, taking initial values of the meson fields $(\sigma, \omega_0, \rho_{0,3})$ as well as the neutron and electron chemical potentials (μ_n, μ_e), the particle densities and Fermi momenta for electrons (k_e, ρ_e), protons (k_p, ρ_p), and hyperons (k_h, ρ_h) can be obtained via the eigenvalues in Eq. (16), chemical equilibriums and charge-neutral conditions in Eqs. (22) and (24), which in turn fix the neutron density ρ_n from baryon number conservations Eq. (23).

(2) With the particle densities (ρ_B, ρ_e, and ρ_μ) and Fermi momenta (k_B, k_e, and k_μ), the meson fields $(\sigma, \omega_0, \rho_{0,3})$ can be obtained from Eqs. (13)–(15).

(3) These two steps should be repeated by iteration until the self-consistence is achieved.

A. Effective interaction strengths in nuclear matter and neutron stars

Using the nonlinear RMF interactions NL1, NL2 [5], NL3 [6], NLSH [7], TM1, TM2 [8], and GL-97 [17] and the density-dependent interactions TW-99 [9], and DD-ME1 [10], the density dependencies of various effective interaction strengths in RMF theory are studied and carefully compared in nuclear matter and neutron stars.

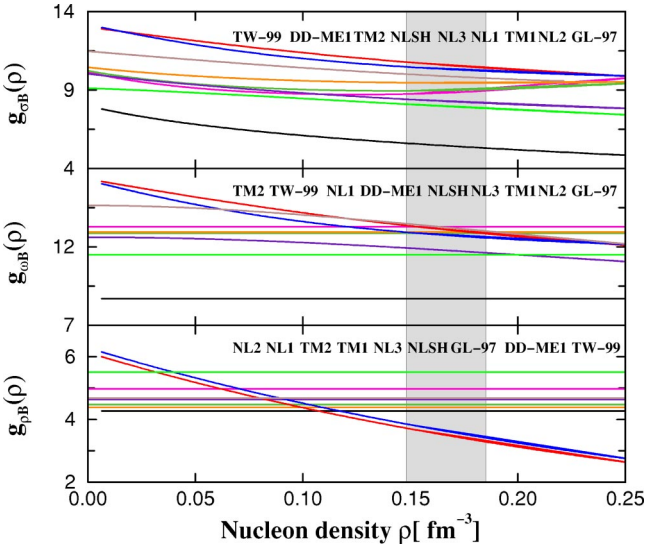

FIG. 1. (Color online) The effective interaction strengths for σ (top), ω (middle), and ρ (bottom) in symmetric nuclear matter as functions of the nucleon density. The shadowed area corresponds to the empirical value of the saturation density in nuclear matter (Fermi momentum $k_F=1.35\pm0.05$ fm^{-1} or density $\rho=0.166\pm0.018$ fm^{-3}). The curves are labeled from the top to the bottom at $\rho=0.15$ fm^{-3} orderly from left to right.

In Fig. 1, the density dependencies of the effective interaction strengths for σ (top), ω (middle) and ρ (bottom) mesons in symmetric nuclear matter as functions of the nucleon density are shown. The shadowed area corresponds to the empirical value of the saturation density in nuclear matter (Fermi momentum $k_F=1.35\pm0.05$ fm^{-1} or density $\rho=0.166\pm0.018$ fm^{-3}). These curves are labeled from the top to the bottom at $\rho=0.15$ fm^{-3} orderly from left to right. For the nonlinear effective interaction, the "equivalent" density dependencies of the effective interaction strengths for σ, ω, and ρ are extracted from the meson field equations Eqs. (13)–(15) according to

$$g_{\sigma B}(\rho) = g_{\sigma B} + U'(\sigma)/\rho_s = g_{\sigma B} + (g_2\sigma^2 + g_3\sigma^3)/\rho_s, \quad (27)$$

$$g_{\omega B}(\rho) = g_{\omega B} - U'(\omega_0)/\rho = g_{\omega B} - (c_3\omega_0^3)/\rho, \quad (28)$$

$$g_{\rho B}(\rho) = g_{\rho B}. \quad (29)$$

The density dependencies of the interaction strengths for TW-99 and DD-ME1 are very similar for symmetric nuclear matter in Fig. 1, as noted in Ref. [10]. Here the comparison between the nonlinear and the density-dependent interaction will be emphasized.

For the σ meson, the interaction strengths given by TW-99 and DD-ME1 are quite different from the others in either magnitudes or slopes. In particular, strengths of TW-99 and DD-ME1 for the density interval in Fig. 1 are almost twice as large as that of GL-97. Differences for nonlinear and density-dependent interactions can also be seen in the region of the empirical nuclear matter densities. For the ω meson, except TW-99, DD-ME1, TM1, and TM2, all the other strengths are density independent. All the strengths are simi-

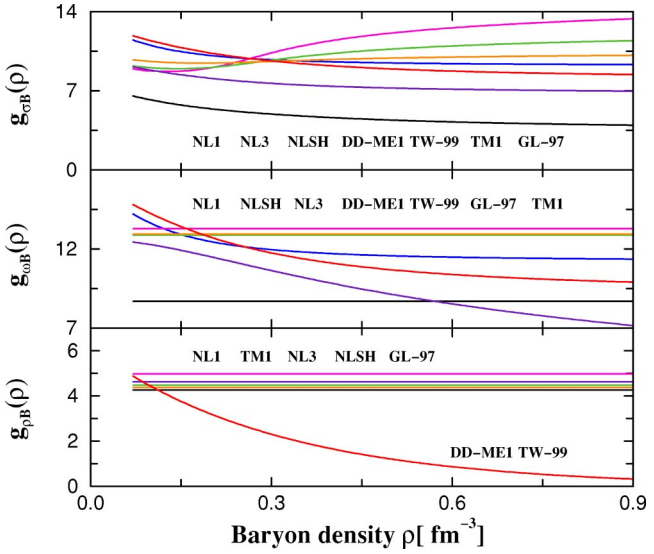

FIG. 2. (Color online) Similar as Fig. 1, but for neutron stars. The curves are labeled from the top to the bottom at $\rho=0.9$ fm^{-3} orderly from left to right.

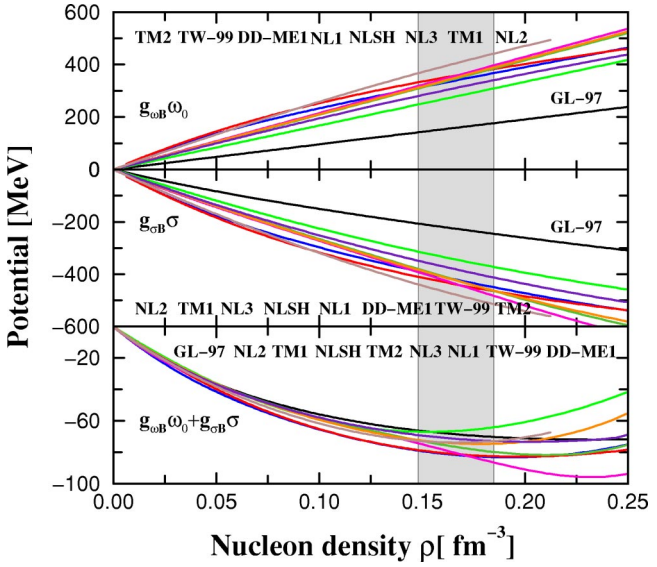

FIG. 3. (Color online) Vector potentials $g_{\omega B}\omega_0$ (top), scalar potentials $g_{\sigma B}\sigma$ (middle), and the sum of both (bottom) in symmetric nuclear matter for different effective interactions (as marked in the figure) as functions of the nucleon density ρ. The shadowed area corresponds to the empirical value of the saturation density in nuclear matter. The curves are labeled from the top to the bottom at $\rho=0.15$ fm^{-3} orderly from left to right.

lar to each other in the region of the empirical saturation densities compared with those of the σ meson, although large differences can also be seen at low densities. For the ρ meson which describes the isospin asymmetry, the strengths for TW-99 and DD-ME1 show strong density dependencies in contrast with the constants in the other interactions. They cross the nonlinear interactions at a density much lower than the empirical saturation density.

The interaction strengths as functions of baryon density for neutron stars matter are given in Fig. 2. As the effective interactions NL2 and TM2 are mainly used in light nuclei, we don't discuss them here. At densities $\rho<0.2$ fm^{-3}, Fig. 2 is similar to Fig. 1. For the scalar σ-meson, the interaction strengths of TW-99, DD-ME1, TM1, and GL-97 decrease with the baryon density in similar slopes, while those of NL1, NL3, and NLSH decrease with baryon density for the densities $\rho<0.2$ fm^{-3}, then increase afterwards. This is due to the positive $g_3\sigma^3$ in Eq. (27) for NL1, NL3, and NLSH, in contrast with the negative ones for TM1 and GL-97. For the vector ω meson, the interaction strengths of TW-99, DD-ME1, and TM1 decrease with the baryon density. At densities $0.2<\rho<0.55$ fm^{-3}, the strengths of DD-ME1, TW-99, and TM1 are between those of NL3 and GL-97. The curve given by TM1 crosses with the line of GL-97 at density $\rho\approx0.57$ fm^{-3}, and then gives the weakest interaction strength. For isospin-vector ρ meson, the interaction strengths of TW-99 and DD-ME1 decrease with baryon density and trend to vanish at high densities, while the others are constants.

Although the aspects of the interaction strengths are quite different from each other, as it will be shown in the following sections, all of them give fair descriptions for the properties of nuclear matter.

B. Potentials for nuclear matter and neutron stars

Potentials for symmetric nuclear matter, pure neutron matter and neutron stars calculated with density-dependent interactions TW-99 and DD-ME1 are illustrated in Figs. 3–5. The results are shown in comparison with those obtained with the nonlinear interactions, such as NL1, NL2, NL3, NLSH, TM1, TM2, and GL-97.

As the contribution of ρ-meson potential for symmetric nuclear matter vanishes, we show the vector potentials $g_{\omega B}\omega_0$, scalar potentials $g_{\sigma B}\sigma$ and their sum as functions of nucleon density ρ for different effective interactions which are marked from top to bottom at density $\rho=0.15$ fm^{-3} orderly from left to right in Fig. 3. For the vector and scalar potentials, GL-97 gives the weakest results due to its weakest interaction strength in Fig. 1. The curves associated with the other interactions lie between those by TM2 and NL2. Their difference increases with the density, the difference of scalar potentials at $\rho=0.15$ fm^{-3} between NL2 and TM2 is around 120 MeV, and that of vector potentials is around 130 MeV. At saturation density, the scalar and vector potentials given by the density-dependent interactions TW-99 and DD-ME1 are similar to the nonlinear interactions except for GL-97, TM2, and NL2. For the total potentials for symmetric nuclear matter $g_{\omega B}\omega_0+g_{\sigma B}\sigma$, GL-97 also gives the weakest result and the difference for different interactions is about 20–30 MeV in the range of saturated densities.

The vector potentials $g_{\omega B}\omega_0$, scalar potentials $g_{\sigma B}\sigma$, isospin potentials $g_{\rho B}\rho_{0,3}$, and their sum as functions of the nucleon density for different effective interactions are shown in Fig. 4 for pure neutron matter. The variations of the vector potentials with density ρ are same as those for symmetric nuclear matter because they are related to the whole nucleon density ρ only. The variations of the scalar potentials with density ρ are slightly different from those for symmetric nuclear matter, as the same density for symmetric nuclear matter and pure neutron matter implicates different Fermi

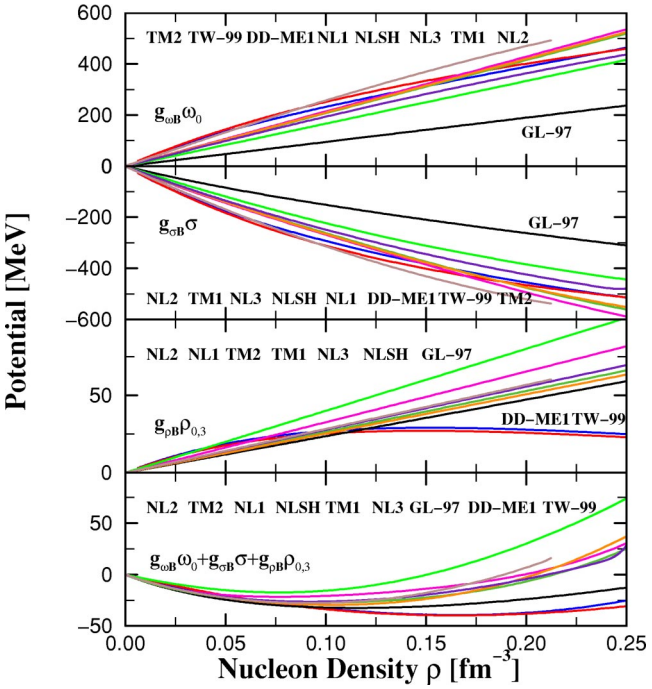

FIG. 4. (Color online) Vector potentials $g_{\omega B}\omega_0$, scalar potentials $g_{\sigma B}\sigma$, isospin vector potentials $g_{\rho B}\rho_{0,3}$, and the sum of them in pure neutron matter for different effective interactions as functions of the nucleon density ρ. The curves are labeled from the top to the bottom at $\rho=0.15$ fm^{-3} orderly from left to right.

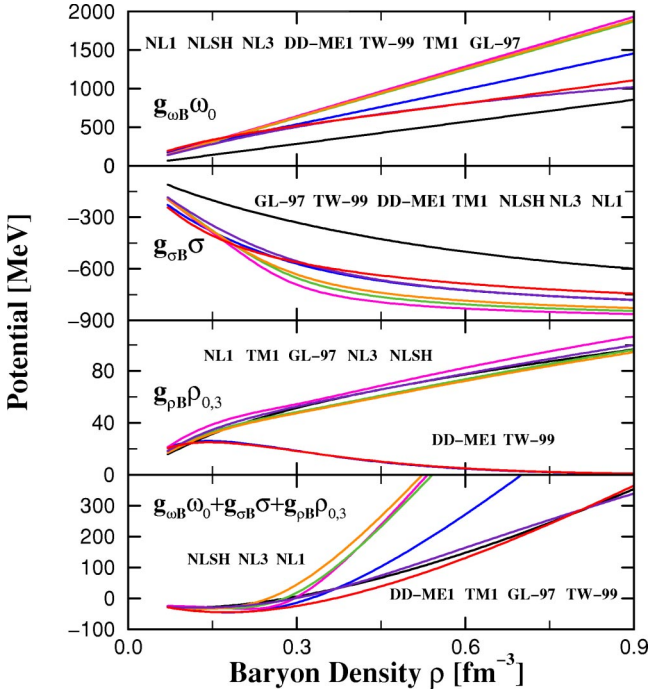

FIG. 5. (Color online) Vector potentials $g_{\omega B}\omega_0$, scalar potentials $g_{\sigma B}\sigma$, isospin vector potentials $g_{\rho B}\rho_{0,3}$, and the sum of them in neutron stars with neutrons and protons only, for different effective interactions as functions of the baryon density ρ. The curves are labeled from the top to the bottom at $\rho=0.45$ fm^{-3} orderly from left to right.

momentum, k_B, as shown in Eq. (18). The ρ meson provides the necessary isospin asymmetry. In pure neutron matter, the isospin potentials $g_{\rho B}\rho_{0,3}$ given by nonlinear interactions increase linearly with the density due to their constant interaction strengths in Fig. 1. While for the same reasons, we can easily understand the isospin potentials for the density-dependent interactions. The compensation between the density dependencies of $g_{\rho B}$ and the increase of the density makes the isospin potentials increase at first and decrease after $\rho=0.12$ fm^{-3}. The sum of the vector potentials $g_{\omega B}\omega_0$, scalar potentials $g_{\sigma B}\sigma$, and isospin potentials $g_{\rho B}\rho_{0,3}$ gives the total potentials for baryon in pure neutron matter. The total potentials are attractive at low densities and become repulsive at high densities. Different from those of symmetric nuclear matter, due to the contribution of the isospin potentials for pure neutron matter, the difference between the total potentials is quite large, e.g., the largest difference 40 MeV between NL2 and TW-99 occurs at $\rho=0.15$ fm^{-3}.

For neutron stars, Fig. 5 shows the vector potentials $g_{\omega B}\omega_0$, scalar potentials $g_{\sigma B}\sigma$, iso-vector potentials $g_{\rho B}\rho_{0,3}$ and the sum of them for different effective interactions as functions of the baryon density ρ. For scalar and vector potentials at densities $\rho<0.2$ fm^{-3}, the properties are similar to those in Figs. 3 and 4. The vector potentials $g_{\omega B}\omega_0$, which offer short-range repulsive interactions, increase with the baryon density, while the scalar potentials $g_{\sigma B}\sigma$, which offer medium-range attractive interactions, change evidently at densities $\rho<0.3$ fm^{-3}, and reach saturation at density $\rho\approx 0.4$ fm^{-3}. Just as for nuclear matter, GL-97 always gives the weakest scalar and vector potentials. Due to the strong interaction strengths of NL1, NL3, and NLSH at high densities as shown in Fig. 2, they give large scalar and vector potentials at densities $\rho>0.3$ fm^{-3}. The results calculated with DD-ME1, TW-99, and TM1 lie in the middle. The difference in potentials between the two density-dependent effective interactions DD-ME1 and TW-99 shows up clearly beyond the density $\rho=0.4$ fm^{-3}, in contrast with that for nuclear matter.

As shown in Fig. 5, the contribution of the ρ-meson provides the necessary isospin asymmetry for neutron stars. For densities $0.065<\rho<0.1$ fm^{-3}, the potential $g_{\rho B}\rho_{0,3}$ calculated with various interactions range from 20 MeV to 30 MeV. For nonlinear interactions, the potentials $g_{\rho B}\rho_{0,3}$ increase with the baryon density and are about 100 MeV at density $\rho=0.9$ fm^{-3}, which are about 10% of the vector potentials $g_{\omega B}\omega_0$ for GL-97 and TM1, and 5% of those for NL1, NL3, and NLSH. For density-dependent interactions, the isospin potentials trend to vanish after $\rho=0.75$ fm^{-3}, due to the density dependencies of the ρ-meson interaction strengths in Fig. 2.

The total potentials $g_{\omega B}\omega_0+g_{\sigma B}\sigma+g_{\rho B}\rho_{0,3}$ are attractive at low densities. At high densities, they become repulsive and the neutron stars are bound by the gravity. The results given by various interactions are similar at densities $\rho<0.2$ fm^{-3} and become quite different at $\rho>0.3$ fm^{-3}. The total potentials for NL1, NL3 and NLSH are close to each other and increase rapidly. Those for TW-99, GL-97, and TM1 are close to each other after $\rho\simeq 0.16$ fm^{-3}, while that of DD-ME1 lies in between.

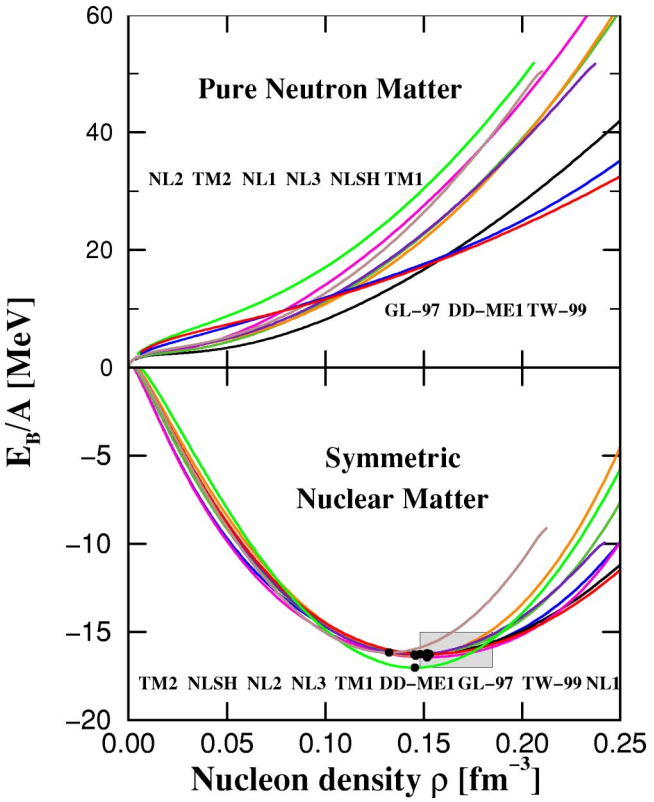

FIG. 6. (Color online) Energies per nucleon, $E_B/A=\varepsilon/\rho-m$, in pure neutron matter (upper panel) and symmetric nuclear matter (lower panel) for different effective interactions as functions of nucleon density ρ. The dots in the lower panel correspond to the saturation densities in symmetric nuclear matter and the shadowed area corresponds to the empirical value of saturation densities in symmetric nuclear matter (density $\rho=0.166\pm0.018$ fm^{-3} and energy per particle $\varepsilon/\rho=-16.0\pm1.0$ MeV). The curves are labeled from the top to the bottom at $\rho=0.2$ fm^{-3} orderly from left to right.

C. Properties of nuclear matter

In Fig. 6 we display the energies per nucleon, $E_B/A=\varepsilon/\rho-m$, for pure neutron matter (upper panel) and symmetric nuclear matter (lower panel) for density-dependent interactions TW-99 and DD-ME1 as functions of nucleon density ρ. For comparison, the results for various nonlinear interactions are also shown. We label the curves from top to bottom at density $\rho=0.20$ fm^{-3} orderly from left to right.

In the upper panel of Fig. 6, the energies per nucleon for all interactions are always positive and increase with the nucleon density for pure neutron matter. The results for density-dependent interactions DD-ME1 and TW-99 are very similar to each other. At densities $\rho<0.075$ fm^{-3}, they are larger than the other interactions except for NL2, thereafter they cross the curves for the other interactions and give the smallest energy per nucleon after densities $\rho>0.17$ fm^{-3}.

For symmetric nuclear matter, the curves for energies per nucleon for various interactions display similar dependencies on densities below the saturation density and pronounced differences at higher densities. The saturation densities for various interactions are similar ($\rho=0.166\pm0.018$ fm-1, $EB/A=-16.33\pm0.10$ MeV) and are located in the empirical range of saturation density except those of TM2 and NL2, which are mainly used for light nuclei.

From the upper and lower panels of Fig. 6, it can be seen that the equations of state at low densities (below saturation density) for pure neutron matter and symmetric nuclear matter are different. The deviations of energy per nucleon E_B/A for symmetric nuclear matter below saturation density are negligible compared with those for pure neutron matter (the deviation is about 15 MeV at density $\rho=0.15$ fm^{-3}). The different results for symmetric nuclear matter and pure neutron matter mainly come from the potentials as shown in Figs. 3 and 4, especially from the isospin potentials $g_{\rho B}\rho_{0,3}$, which exhibits large deviation.

From Fig. 3, we have seen that the difference for the total potentials at saturated density in symmetric nuclear matter is about $20\sim30$ MeV, while the energies per nucleon at saturation density are close to each other in Fig. 6. To understand these, we will discuss energy per nucleon at the saturation density for symmetric nuclear matter in detail.

From Eq. (19) and the meson field equations Eqs. (13)–(15), the energy density for symmetric nuclear matter can be expressed as

$$\begin{aligned}\varepsilon &= \frac{1}{2}m_\sigma^2\sigma^2 + U(\sigma) - \frac{1}{2}m_\omega^2\omega_0^2 - U(\omega_0) - \sum_B \rho_B\Sigma_{0B}^R \\ &+ \left[m_\omega^2\omega_0^2 + 4U(\omega_0) + \sum_B \rho_B\Sigma_{0B}^R \right. \\ &\left. + \frac{1}{\pi^2}\sum_B \int_0^{k_B} k^2 dk\sqrt{k^2+(m_B+g_{\sigma B}\sigma)^2} \right] \\ &= -\frac{1}{2}g_{\sigma B}\sigma\rho_s - \frac{1}{6}g_2\sigma^3 - \frac{1}{4}g_3\sigma^4 - \frac{1}{2}g_{\omega B}\omega_0\rho \\ &+ \frac{1}{4}c_3\omega_0^4 - \sum_B \rho_B\Sigma_{0B}^R + \left[g_{\omega B}\omega_0\rho + \sum_B \rho_B\Sigma_{0B}^R \right. \\ &\left. + \frac{1}{\pi^2}\sum_B \int_0^{k_B} k^2 dk\sqrt{k^2+(m_B+g_{\sigma B}\sigma)^2} \right] \\ &= \varepsilon_\sigma + \varepsilon_\omega + \varepsilon_{re} + \varepsilon_N, \end{aligned} \tag{30}$$

where,

$$\varepsilon_\sigma = -\frac{1}{2}g_{\sigma B}\sigma\rho_s - \frac{1}{6}g_2\sigma^3 - \frac{1}{4}g_3\sigma^4, \tag{31}$$

$$\varepsilon_\omega = -\frac{1}{2}g_{\omega B}\omega_0\rho + \frac{1}{4}c_3\omega_0^4, \tag{32}$$

$$\varepsilon_{re} = -\sum_B \rho_B\Sigma_{0B}^R, \tag{33}$$

$$\varepsilon_N^p = g_{\omega B}\omega_0\rho + \sum_B \rho_B\Sigma_{0B}^R, \tag{34}$$

$$\varepsilon_N^k = \frac{1}{\pi^2}\sum_B \int_0^{k_B} k^2 dk\sqrt{k^2+(m_B+g_{\sigma B}\sigma)^2}, \tag{35}$$

TABLE I. The Fermi momenta k_F ($\rho_0=k_F^3/3\pi^2$), vector densities ρ_0, scalar densities ρ_s, scalar potentials $g_{\sigma B}\sigma$, vector potentials $g_{\omega B}\omega_0$, the energy densities ε_σ, ε_ω, ε_{re}, ε_N^p, ε_N^k, and ε_N, the total energy densities ε, nucleon masses m and energies per nucleon $E_B/A=\varepsilon/\rho-m$ for different interactions in symmetric nuclear matter at saturation density (the units are in MeV fm^{-3} except otherwise stating)

	TW-99	DD-ME1	GL-97	NL1	NL2	NL3	NLSH	TM1	TM2
k_F(fm^{-1})	1.313	1.310	1.313	1.310	1.292	1.300	1.293	1.291	1.251
ρ_0(fm^{-3})	0.153	0.152	0.153	0.152	0.146	0.148	0.146	0.145	0.132
ρ_s(fm^{-3})	0.143	0.143	0.148	0.142	0.139	0.140	0.138	0.138	0.125
$g_{\sigma B}\sigma$(MeV)	−417.9	−396.2	−206.4	−400.7	−309.7	−380.3	−378.24	−342.94	−402.06
$-\frac{1}{2}g_{\sigma B}\sigma\rho_s$	29.871	28.279	15.274	28.450	21.524	26.621	26.099	23.663	25.129
ε_σ	29.871	28.279	13.830	28.187	20.538	26.088	25.544	22.387	24.027
$g_{\omega B}\omega_0$(MeV)	338.7	316.7	145.57	325.4	242.9	308.0	306.6	274.5	331.8
$-\frac{1}{2}g_{\omega B}\omega_0\rho_0$	−25.910	−24.069	−11.140	−24.689	−17.688	−22.832	−22.378	−19.901	−21.897
ε_σ	−25.910	−24.069	−11.140	−24.689	−17.688	−22.832	−22.378	−19.408	−21.221
ε_{re}	−0.161	−0.364	0	0	0	0	0	0	0
ε_N^p	51.981	48.502	22.281	49.378	35.375	45.664	44.757	39.856	43.893
ε_N^k	85.401	87.912	116.199	87.207	96.244	87.643	86.786	91.016	75.261
ε_N	137.382	136.414	138.470	136.585	131.619	133.307	131.543	130.872	119.155
ε	141.182	140.260	141.169	140.083	134.470	136.563	134.708	133.649	120.678
m(MeV)	939	939	939	938	938	939	939	938	938
E_B/A(MeV)	−16.25	−16.23	−16.32	−16.42	−17.02	−16.25	−16.35	−16.265	−16.16

$$\varepsilon_N=\varepsilon_N^p+\varepsilon_N^k, \tag{36}$$

in which, the contributions from σ and ω fields are, respectively, ε_σ and ε_ω, the rearrangement term is ε_{re}, and the contribution from nucleons is ε_N with its potential energy part ε_N^p and kinetic energy part ε_N^k. For nonlinear interactions, $\varepsilon_{re}=0$, while for the density-dependent interactions, $g_2=g_3=c_3=0$.

In Table I, the Fermi momenta $k_F(\rho_0=k_F^3/3\pi^2)$, vector densities ρ_0, scalar densities ρ_s, scalar potentials $g_{\sigma B}\sigma$, vector potentials $g_{\omega B}\omega_0$, the various contributions ε_σ, ε_ω, ε_{re}, ε_N^p, ε_N^k, and ε_N, the system energy densities ε, nucleon mass m and energies per nucleon $E_B/A=\varepsilon/\rho-m$ at saturation density for different interactions are shown. The saturation densities given by various interactions are similar ($\rho_0\approx 0.150$ fm^{-3}), except for TM2 ($\rho_0=0.132$ fm^{-3}). From Eqs. (30)–(36), we know that if the scalar densities ρ_s and vector densities ρ_0 (or Fermi momenta k_F) at saturation densities are similar, larger scalar potentials (negative) will give larger ε_σ (positive) and smaller ε_N^k (positive), and larger vector potentials will give larger ε_ω (negative) and ε_N^p (positive). Taking into account the contribution of the rearrangement term ε_{re}, the energies per nucleon $E_B/A=\varepsilon/\rho-m$ for various interactions become closer to each other. For example, for TW-99 and GL-97, which give the largest and smallest potentials, respectively, the difference of $g_{\sigma B}\sigma\sim-210.5$ MeV leads to $\Delta\varepsilon_\sigma=1604$ MeV fm^{-3} and $\Delta\varepsilon_N^k=-30.80$ MeV fm^{-3}, and the difference of $g_{\omega B}\omega\sim 194.1$ MeV leads to $\Delta\varepsilon\omega=-14.77$ MeV fm−3 and $\Delta\varepsilon_N^p=29.70$ MeV fm^{-3}. Taking into account the contribution of the rearrangement term $\Delta\varepsilon_{re}=-0.16$ MeV fm^{-3}, the difference between the total energy densities is $\Delta\varepsilon=0.01$ MeV fm^{-3}, i.e., the difference between their energy per nucleon $\Delta E_B/A=\Delta(\varepsilon/\rho_0-m)=0.07$ MeV, which is small compared with $E_B/A\approx 16$ MeV.

The saturation properties of symmetric nuclear matter for different interactions including the Fermi momenta k_F, saturation densities ρ_0, energies per nucleon E_B/A, effective masses m^* and m^*/m, incompressibility K and symmetric energy coefficients a_{sym} are shown in Table II. We can see that the results given by the density-dependent interactions DD-ME1 and TW-99 are similar to those of the nonlinear interactions except for TM2, NL2, and GL-97. The saturation density for TM2 is lower and the energy per nucleon for NL2 is larger than the corresponding empirical values, which can also be seen in Fig. 6. Due to the weakest scalar potentials shown in the middle panel of Fig. 3, GL-97 gives the largest effective mass $m^*/m=0.78$ and incompressibility $K=240$ MeV, which are justified from the empirical nuclear saturation properties [17].

Although properties below the saturation densities for symmetric nuclear matter are quite similar, the EOS at low densities given by various interactions for pure neutron matter is quite different. This is due to the effective interactions used so far are obtained by fitting the properties of doubly magic nuclei, which have an isospin close to that of the symmetric nuclear matter. To get an EOS for neutron matter without any ambiguity, it is necessary to constrain the effective interactions either by microscopic many-body calculations for the neutron matter data [18] or the data of nuclei with extreme isospin.

D. Properties of neutron stars

The energies per baryon for neutron stars as functions of baryon density for different interactions are given in Fig. 7. At low densities, Fig. 7 is very similar to the top panel of

TABLE II. Nuclear matter saturation properties for different effective interactions, including the Fermi momenta k_F, saturation densities ρ_0, energies per nucleon E_B/A, effective masses m^* and m^*/m, incompressibility K, and symmetric energy coefficients a_{sym}.

	k_F(fm^{-1})	ρ_0(fm^{-3})	E_B/A(MeV)	m^*(MeV)	m^*/m	K(MeV)	a_{sym}(MeV)
DD-ME1	1.310	0.152	−16.23	542.7899	0.578	244.50	33.06
TW-99	1.313	0.153	−16.25	521.0724	0.555	240.00	32.77
NL1	1.310	0.152	−16.42	537.2949	0.573	211.15	43.47
NL2	1.292	0.146	−17.02	628.3138	0.670	399.17	45.12
NL3	1.300	0.148	−16.25	558.6835	0.595	271.73	37.42
NLSH	1.293	0.146	−16.35	560.7559	0.598	355.34	36.12
TM1	1.291	0.145	−16.265	595.0626	0.634	281.17	36.89
TM2	1.251	0.132	−16.16	535.9376	0.571	343.83	35.98
GL-97	1.313	0.153	−16.32	732.6145	0.780	240.00	32.5

Fig. 6 as the neutron stars matter is almost pure neutron matter at low densities. The energies per baryon for the nonlinear interactions NL1, NL3, and NLSH increase quickly with the density compared with those of TW-99 and GL-97, while the results for DD-ME1 and TM1 lie in-between. These results are in consistent with the total potentials for neutron stars in Fig. 5. At density $\rho \sim 0.3$ fm^{-3}, the potentials for TW-99 and DD-ME1 are the lowest, while that of DD-ME1 crosses GL-97 and TM1 at $\rho \sim 0.4$ fm^{-3} in Fig. 5. The E_B/A for TW-99 is the smallest.

The evolutions of particle densities with the baryon density in neutron stars are given in Fig. 8, and the corresponding figures in logarithm scale for low densities ($0.05 < \rho$ fm$^3 < 0.2$) are given in the subfigures, where the solutions are from $\rho = 0.065$ fm^{-3} to 0.9 fm^{-3}, i.e., $0.425 \leqslant \rho_B/\rho_0 \leqslant 5.88$ with $\rho_0 = 0.153$ fm^{-3}.

At low densities, the charge-neutral neutron star matter is mainly composed of neutrons. As the density increases, high-momentum neutrons will β decay into protons and electrons ($n \leftrightarrow p + e^- + \overline{\nu_e}$) until the equilibrium at which the chemical potentials satisfy $\mu_p = \mu_n - \mu_e$. As the neutron density increases, so do the proton and electron densities. When μ_e attains the value of the muon mass, μ^- will appear. The equilibrium with respect to the reaction $e^- \leftrightarrow \mu^- + \overline{\nu_\mu} + \nu_e$ implies that $\mu_e = \mu_\mu$. The μ^- thresholds are different for different effective interactions. All the μ^- thresholds are in the range of $\rho = 0.11 \pm 0.01$ fm^{-3} with the minimum and maximum thresholds given by NL1 and GL-97, respectively.

From Fig. 8, it can also be seen that the density-dependent effective interactions TW-99 and DD-ME1 give the largest neutron densities, and accordingly the smallest proton densities due to the baryon number conservation. This is because the strengths $g_{\rho B}$ for the density-dependent effective interaction become weaker with the baryon density, as shown in Fig. 2. Because of the charge-neutral condition, the densities of electron and μ^- for different effective interactions have the same tendencies as the proton densities.

As hyperons would appear at roughly twice saturation density, it is necessary to study neutron star with hyperons.

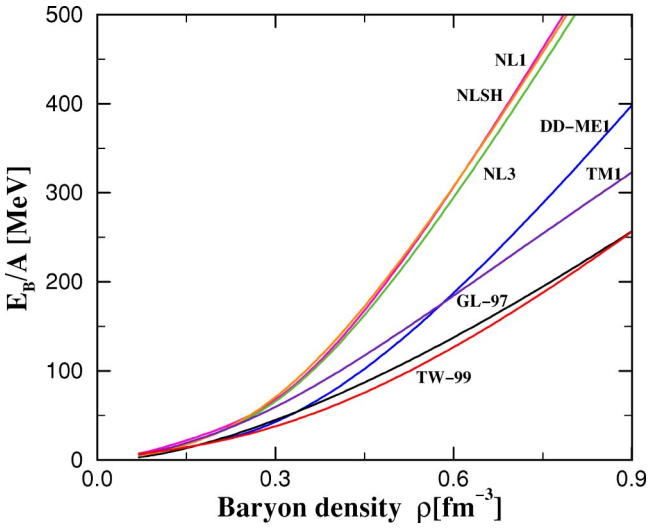

FIG. 7. (Color online) Similar as Fig. 5, but for neutron stars.

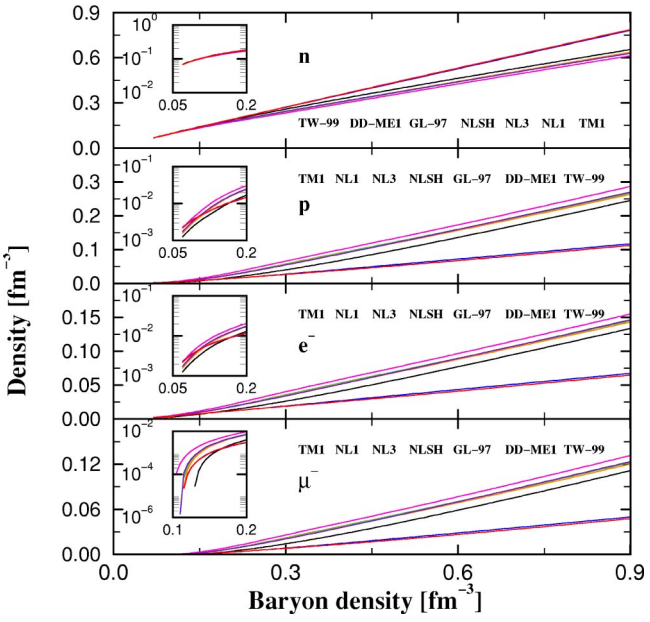

FIG. 8. (Color online) Particle densities (from top to bottom are, respectively, n, p, e^- and μ^-) in neutron stars for different effective interactions as a function of the baryon density ρ. The corresponding inserts are the same figures in a logarithmic scale at low density ($0.05 < \rho$ fm$^3 < 0.2$). The curves are labeled from the top to the bottom at $\rho = 0.45$ fm^{-3} orderly from left to right.

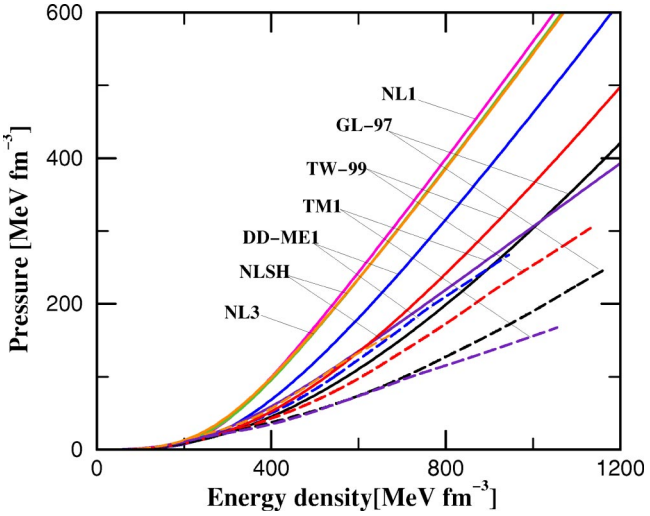

FIG. 9. (Color online) EOS of neutron stars for different effective interactions (as marked in figure). The solid lines represent these with neutrons and protons only, and the dashed lines represent the corresponding ones with hyperons included, respectively.

The details for the inclusion of hyperons in neutron star in relativistic mean field theory are given in Refs. [17,31]. One can introduce the ratios of the meson- hyperons coupling strengths coupling constants to those of nucleons as

$$x_{\sigma h} = \frac{g_{\sigma h}}{g_{\sigma N}}, \quad x_{\omega h} = \frac{g_{\omega h}}{g_{\omega N}}, \quad x_{\rho h} = \frac{g_{\rho h}}{g_{\rho N}}, \tag{37}$$

where, $g_{\sigma h}$, $g_{\omega h}$, and $g_{\rho h}$ have the same density dependencies as $g_{\sigma N}$,$g_{\omega N}$, and $g_{\rho N}$ respectively, and the ratios $x_{\sigma h}=x_{\omega h}=x_{\rho h}=\sqrt{2/3}$ are chosen according to Ref. [32].

The equation of state (EOS) is very important to understand the structure of neutron star. The stiffer the EOS, the larger the mass that can be sustained against collapse. There are two constraints for the realistic EOS. One is a stiff limit by the causal constraint $\partial p/\partial \varepsilon \leqslant 1$, which results in the limit mass of just over $3M_{\odot}$. The other corresponds to the soft limit, which corresponds to the free Fermi gas with neutrons, protons and leptons in equilibrium and the limit mass is about $0.7M_{\odot}$ [17]. Here the EOS calculated by different effective interactions are given in Fig. 9. The solid lines represent these with neutrons and protons only, and the dashed lines represent their corresponding ones with hyperons included, respectively. As can be understood from the potentials in Fig. 5, the nonlinear interactions NL1, NL3, and NLSH give stiffer EOS than the other interactions, GL-97 and TM1 give softer EOS, and density-dependent interactions TW-99 and DD-ME1 lie in between. Furthermore, the inclusion of hyperons softens the corresponding EOS considerably, as shown by the corresponding dashed lines in Fig. 9. The softest EOS is given by TM1. After the inclusion of hyperons, the corresponding solutions for the nonlinear interactions, NL1, NL3, and NLSH, exist only below density, $\rho=0.42, 0.51$, and 0.58 fm^{-3}, respectively. Beyond the corresponding density, the scalar potential $g_{\sigma B}\sigma$ will increase and make the effective masses $m^{*}=m+g_{\sigma B}\sigma$ negative. Therefore

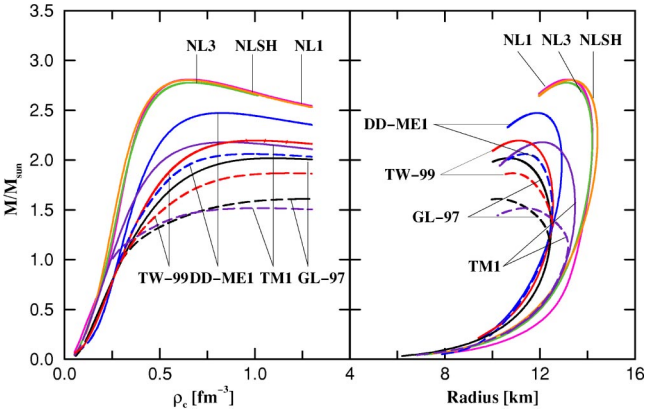

FIG. 10. (Color online) The masses versus the central densities (left panel) and radii (right panel) in neutron stars for different effective interactions (as marked in figure). The solid lines represent these with neutrons and protons only, and the dashed lines represent the corresponding ones with hyperons included.

in the following, we do not discuss the properties of neutron stars with hyperons for NL1, NL3, and NLSH.

For a static global star, the Oppenheimer-Volkoff-Tolman (OVT) equation is [15,16]:

$$\frac{dp}{dr} = -\frac{[p(r)+\varepsilon(r)][M(r)+4\pi r^3 p(r)]}{r[r-2M(r)]}, \tag{38}$$

$$M(r) = 4\pi \int_0^r \varepsilon(r) r^2 dr. \tag{39}$$

The point R, at which the pressure vanishes, $p(R)=0$, defines the radius of the star and $M(R)$ is the gravitational mass. For a given EOS, the OVT equation has a unique solution which depends on a single parameter characterizing the conditions of matter at the center. This can be chosen as the baryon density or energy density. In Fig. 10, the masses versus the central densities (left panel) and radii (right panel) of neutron stars for different interactions are shown. The solid lines represent these with neutrons and protons only, and the dashed lines represent the corresponding ones with hyperons included. There is critical maximum value for the masses of neutron star, known as the OV mass limit. Beyond this mass the star is unstable to gravitational collapse.

The OV mass limits, corresponding radii, central densities, energy densities, and pressures for different effective interactions are presented in Table III. The second rows for DD-ME1, TW-99, GL-97, and TM1 represent the quantities with hyperons. Without hyperons, the OV mass limits calculated from different EOS are $(2.02-2.81)M_{\odot}$, and the corresponding radii are 10.24–13.27 km. The OV mass limits and corresponding radii for DD-ME1 and TW-99 are, respectively, $2.475M_{\odot}$,11.903 km and $2.195M_{\odot}$,11.209 km and they give softer EOS and smaller OV mass limits than those of the effective interactions NL1 ($2.809M_{\odot}$,13.137 km), NL3 ($2.778M_{\odot}$,13.081 km), and NLSH ($2.803M\odot$, 13.270 km). The results for TM1 are similar to TW-99,

TABLE III. The central densities, energy densities, and pressures, OV mass limits and corresponding radii for neutron stars for different effective interactions. For interactions DD-ME1, TW-99, TM1, and GL-97, the same quantities for neutron stars with hypersons are given in the following lines, respectively.

	Central density (fm^{-3})	Central energy density ($\times 10^{15}$ g/cm^3)	Central pressure ($\times 10^{35}$ dyne/cm^2)	OV mass limit ($\times M_\odot$)	Radius (km)
DD-ME1	0.815	1.852	7.886	2.475	11.903
	0.980	2.097	5.780	2.061	11.375
TW-99	0.970	2.126	7.902	2.195	11.209
	1.176	2.422	6.318	1.868	10.853
TM1	0.852	1.881	5.293	2.180	12.054
	1.016	2.083	3.071	1.517	11.366
GL-97	1.045	2.347	7.905	2.018	10.779
	1.299	2.792	6.188	1.610	10.242
NL1	0.658	1.529	7.140	2.809	13.137
NL3	0.667	1.544	7.055	2.778	13.081
NLSH	0.649	1.497	6.682	2.803	13.270

while GL-97 gives the smallest OV mass limit ($2.018M_\odot$) and radius (10.779 km).

Due to the softer EOS for neutron star with hyperons, small OV mass limits have been obtained. The OV mass limits calculated with hyperons for DD-ME1, TW-99 GL-97 and TM1 are $(1.52-2.06)M_\odot$, and the corresponding radii are 10.24–11.38 km. With hyperons included, the OV mass limits and corresponding radii for DD-ME1 and TW-99 are, respectively, $2.061M_\odot$, 11.375 km and $1.868M_\odot$, 10.853 km. The results for TM1 are similar to TW-99, and give radius (11.366 km) and the smallest OV mass limit ($1.517M_\odot$).

IV. SUMMARY

We have studied and carefully compared the density dependencies of various effective interaction strengths in symmetric nuclear matter, pure neutron matter, and neutron stars. The corresponding influences on potentials and properties of symmetric nuclear matter, pure neutron matter, and neutron stars are presented and discussed. As the interactions NL2 and TM2 are aimed for light nuclei, we don't present their results for neutron star. The properties calculated by the interactions NL1, NL3, and NLSH are close to each other. The same conclusion can be seen for the density-dependent interactions TW-99 and DD-ME1.

For the σ meson, all the interaction strengths are density dependent. While for the ω meson, TW-99, DD-ME1, and TM1 are density dependent. For the ρ meson, the interaction strengths for TW-99 and DD-ME1 decrease very fast with density while the others are constant. Even though the interaction strengths and the potentials from various interactions are different, the differences of saturation properties for various effective interactions in symmetric nuclear matter are subtle except for NL2 and TM2.

Unlike those for symmetric nuclear matter, the properties for pure neutron matter by various interactions are quite different. As the effective interactions used so far are obtained by fitting the properties of doubly magic nuclei, it may be successful for nuclear matter with an isospin close to that of the symmetric nuclear matter. To get an EOS for neutron matter without any ambiguity, it is necessary to constrain the effective interactions either by microscopic many-body calculations for the neutron matter data or the data of nuclei with extreme isospin.

For neutron star matter, the density-dependent interactions DD-ME1 and TW-99 favor large neutron populations due to their weak ρ-meson field at high densities. The OV mass limits calculated from different EOS are $2.02-2.81M_\odot$, and the corresponding radii are 10.78–13.27 km. The stronger interaction gives a stiffer EOS and a larger mass limit. TW-99 and DD-ME1 give softer EOS and smaller OV mass limits than those of the effective interactions NL1, NL3, and NLSH. The results of TM1 are similar to TW-99. After the inclusion of hyperons, the corresponding values become $1.52-2.06M_\odot$ and 10.24–11.38 km.

ACKNOWLEDGMENTS

We would like to express our gratitude to G. C. Hillhouse for his careful reading of the manuscript. This work is partly supported by the Major State Basic Research Development Program under Contract No. G2000077407 and the National Natural Science Foundation of China under Grant Nos. 10025522, 10221003, and 10047001.

[1] J. D. Walecka, Ann. Phys. (N.Y.) **83**, 491 (1974).
[2] P. Ring, Prog. Part. Nucl. Phys. **37**, 193 (1996).
[3] J. Meng, Nucl. Phys. **A635**, 3 (1998); J. Meng and P. Ring, Phys. Rev. Lett. **77**, 3963 (1996).
[4] J. Meng and P. Ring, Phys. Rev. Lett. **80**, 460 (1998); J. Meng, I. Tanihata, and S. Yamaji, Phys. Lett. B **419**, 1 (1998); J. Meng, H. Toki, J. Y. Zeng, S. Q. Zhang, and S. G. Zhou, Phys. Rev. C **65**, 041302 (2002); J. Meng, S. G. Zhou, and I. Tanihata, Phys. Lett. B **532**, 209 (2002).
[5] Lee Suk-Joon, J. Fink, A. B. Balantekin, M. R. Strayer, A. S. Umar, P. G. Reinhard, J. A. Maruhn, and W. Greiner, Phys. Rev. Lett. **57**, 2916 (1986).
[6] G. A. Lalazissis, J. Konig, and P. Ring, Phys. Rev. C **55**, 540 (1997).
[7] M. M. Sharma, M. A. Nagarajan, and P. Ring, Phys. Lett. B **312**, 377 (1993).
[8] Y. Sugahara and H. Toki, Nucl. Phys. **A579**, 557 (1994).
[9] S. Typel and H. H. Wolter, Nucl. Phys. **A656**, 331 (1999).
[10] T. Nikšić, D. Vretenar, P. Finelli, and P. Ring, Phys. Rev. C **66**, 024306 (2002).
[11] W. Baade and F. Zwicky, Proc. Natl. Acad. Sci. U.S.A. **20**, 255 (1934).
[12] A. Hewish, S. J. Bell, J. D. H. Pikington, P. F. Scott, and R. Collins, Nature (London) **217**, 709 (1968).
[13] F. Pacini, Nature (London) **216**, 567 (1967).
[14] T. Gold, Nature (London) **221**, 25 (1969).
[15] J. R. Oppenheimer and G. M. Volkoff, Phys. Rev. **55**, 374 (1939).
[16] R. C. Tolman, Phys. Rev. **55**, 364 (1939).
[17] N. K. Glendenning, *Compact Stars* (Springer-Verlag, New York, 1997).
[18] H. Heiselberg and M. Hjorth-Jensen, Phys. Rep. **328**, 237 (2000).
[19] H. Madokoro, J. Meng, M. Matsuzaki, and S. Yamaji, Phys. Rev. C **62**, 061301 (2000).
[20] D. B. Kaplan and A. E. Nelson, Phys. Lett. B **175**, 57 (1986).
[21] H. Fujii, T. Maruyama, T. Muto, and T. Tatsumi, Nucl. Phys. **A597**, 645 (1996).
[22] N. K. Glendenning and J. Schaffner-Bielich, Phys. Rev. Lett. **81**, 4564 (1998).
[23] N. K. Glendenning and J. Schaffner-Bielich, Phys. Rev. C **60**, 025803 (1999).
[24] J. A. Pons, S. Reddy, P. J. Ellis, M. Prakash, and J. M. Lattimer, Phys. Rev. C **62**, 035803 (2000).
[25] T. Norsen and S. Reddy, Phys. Rev. C **63**, 065804 (2001).
[26] T. Norsen, Phys. Rev. C **65**, 045805 (2002).
[27] H. Y. Jia, B. X. Sun, J. Meng, and E. G. Zhao, Chin. Phys. Lett. **18**, 1517 (2001).
[28] H. Y. Jia, H. F. Lü, and J. Meng, High Energy Phys. Nucl. Phys. **26**, 1050 (2002) (in Chinese).
[29] B. X. Sun, H. Y. Jia, J. Meng, and E. G. Zhao, Commun. Theor. Phys. **36**, 446 (2001).
[30] H. Y. Jia, J. Meng, E. G. Zhao, J. Li, and J. P. Sang, High Energy Phys. Nucl. Phys. **27**, 200 (2003) (in Chinese).
[31] M. Prakash, I. Bombaci, M. Prakash, P. J. Ellis, J. M. Lattimer, and R. Knorren, Phys. Rep. **280**, 1 (1997).
[32] S. A. Moszkowski, Phys. Rev. D **9**, 1613 (1974).